ACCOUNTS of chemical research

pubs.acs.org/accounts Article

Biomimetic Metal-Free Hydride Donor Catalysts for CO_2 Reduction

Stefan Ilic, Jonathan L. Gesiorski, Ravindra B. Weerasooriya, and Ksenija D. Glusac*

Cite This: *Acc. Chem. Res.* 2022, 55, 844–856 Read Online

ACCESS | Metrics & More | Article Recommendations

CONSPECTUS: The catalytic reduction of carbon dioxide to fuels and value-added chemicals is of significance for the development of carbon recycling technologies. One of the main challenges associated with catalytic CO_2 reduction is product selectivity: the formation of carbon monoxide, molecular hydrogen, formate, methanol, and other products occurs with similar thermodynamic driving forces, making it difficult to selectively reduce CO_2 to the target product. Significant scientific effort has been aimed at the development of catalysts that can suppress the undesired hydrogen evolution reaction and direct the reaction toward the selective formation of the desired products, which are easy to handle and store. Inspired by natural photosynthesis, where the CO_2 reduction is achieved using NADPH cofactors in the Calvin cycle, we explore biomimetic metal-free hydride donors as catalysts for the selective reduction of CO_2 to formate. Here, we outline our recent findings on the thermodynamic and kinetic parameters that control the hydride transfer from metal-free hydrides to CO_2. By experimentally measuring and theoretically calculating the thermodynamic hydricities of a range of metal-free hydride donors, we derive structural and electronic factors that affect their hydride-donating abilities. Two dominant factors that contribute to the stronger hydride donors are identified to be (i) the stabilization of the positive charge formed upon HT via aromatization or by the presence of electron-donating groups and (ii) the destabilization of hydride donors through the anomeric effect or in the presence of significant structural constrains in the hydride molecule. Hydride donors with appropriate thermodynamic hydricities were reacted with CO_2, and the formation of the formate ion (the first reduction step in CO_2 reduction to methanol) was confirmed experimentally, providing an important proof of principle that organocatalytic CO_2 reduction is feasible. The kinetics of hydride transfer to CO_2 were found to be slow, and the sluggish kinetics were assigned in part to the large self-exchange reorganization energy associated with the organic hydrides in the DMSO solvent. Finally, we outline our approaches to the closure of the catalytic cycle via the electrochemical and photochemical regeneration of the hydride (R–H) from the conjugate hydride acceptors (R^+). We illustrate how proton-coupled electron transfer can be efficiently utilized not only to lower the electrochemical potential at which the hydride regeneration takes place but also to suppress the unwanted dimerization that neutral radical intermediates tend to undergo. Overall, this account provides a summary of important milestones achieved in organocatalytic CO_2 reduction and provides insights into the future research directions needed for the discovery of inexpensive catalysts for carbon recycling.

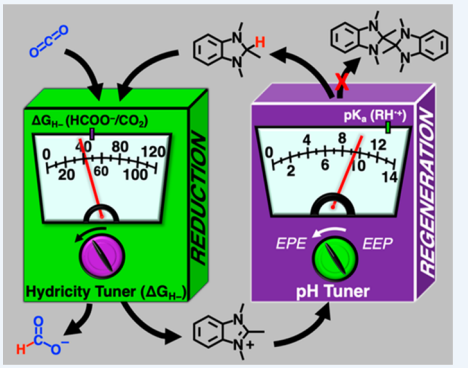

KEY REFERENCES

- Ilic, S.; Pandey Kadel, U.; Basdogan, Y.; Keith, J. A.; Glusac, K. D. Thermodynamic Hydricities of Biomimetic Organic Hydride Donors. *J. Am. Chem. Soc.* **2018**, *140*, 4569–4579.[1] *This study investigates the thermodynamic hydricities of metal-free hydride donors. Electronic and structural factors, such as aromatization, charge delocalization of the conjugate hydride acceptor, and hyperconjugation, were identified as parameters that contribute to hydride ion release.*
- Lim, C.-H.; Ilic, S.; Alherz, A.; Worrell, B. T.; Bacon, S. S.; Hynes, J. T.; Glusac, K. D.; Musgrave, C. B. Benzimidazoles as Metal-Free and Recyclable Hydrides for CO_2 Reduction to Formate. *J. Am. Chem. Soc.* **2019**, *141*, 272–280.[2] *This study demonstrates that the reduction of CO_2 to formate can be achieved by a hydride transfer from benzimidazole-based hydride donors. The formate formation has been quantified, and the electrochemical recycling of the hydride has been demonstrated.*
- Weerasooriya, R. B.; Gesiorski, J. L.; Alherz, A.; Ilic, S.; Hargenrader, G. N.; Musgrave, C. B.; Glusac, K. D. Kinetics of Hydride Transfer from Catalytic Metal-Free Hydride Donors to CO_2. *J. Phys. Chem. Lett.* **2021**, *12*, 2306–2311.[3] *This study investigates the kinetic aspects of hydride transfer from organic hydrides to CO_2. The Marcus*

Received: November 18, 2021
Published: February 24, 2022

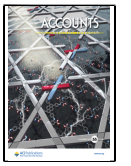

https://doi.org/10.1021/acs.accounts.1c00708
Acc. Chem. Res. 2022, 55, 844–856

Scheme 1. Catalytic CO_2 Reduction by (a) Transition-Metal Complexes, (b) the NADPH Cofactor in Natural Photosynthesis, and (c) Biomimetic NADPH Analogs[a]

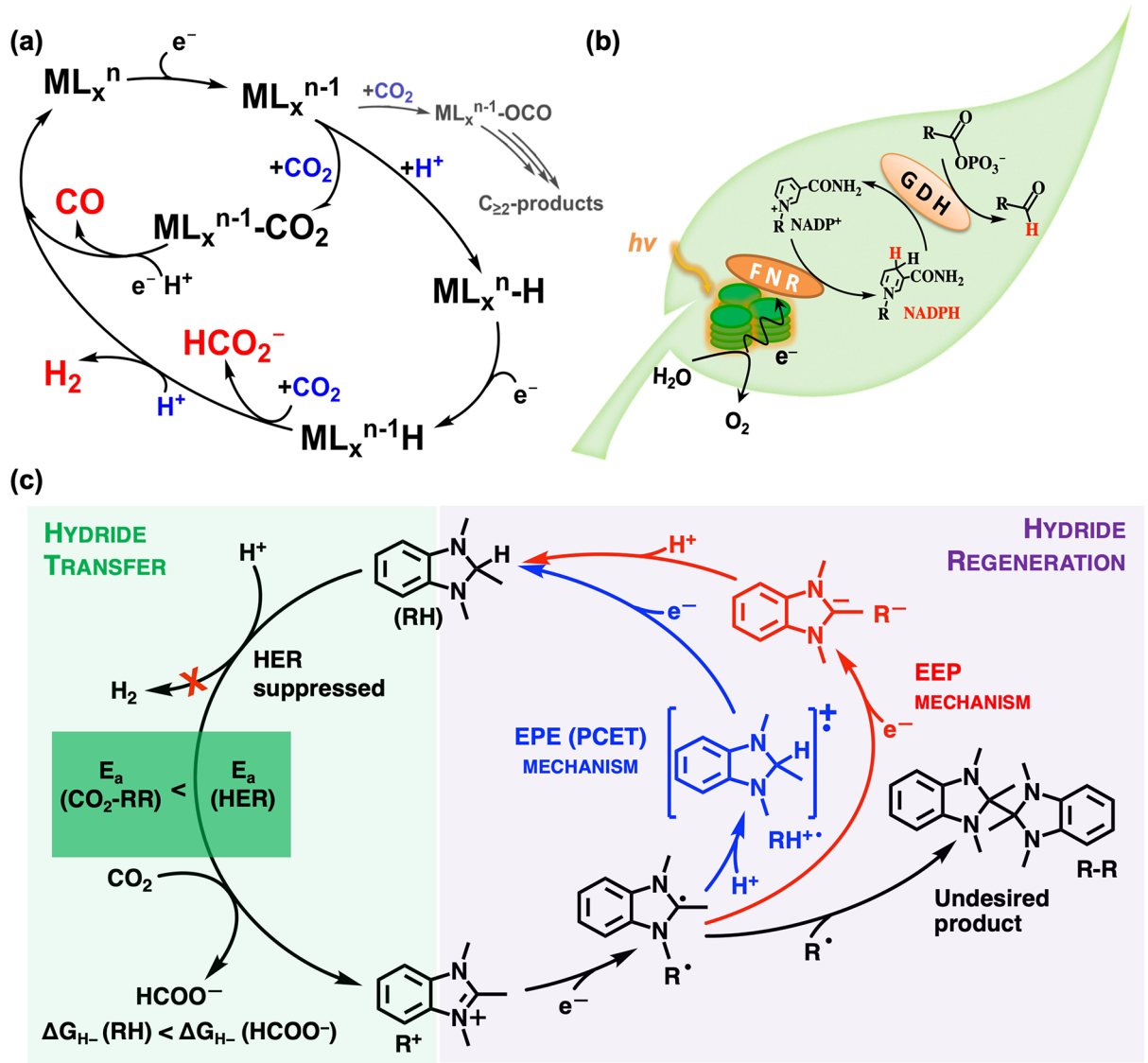

[a]The catalytic cycle is divided into the hydride-transfer (green) and hydride-regeneration (purple) steps.

formalism shows that the reaction kinetics are sluggish due to the large self-exchange reorganization energy associated with the organic hydride donors.

- Ilic, S.; Alherz, A.; Musgrave, C. B.; Glusac, K. D. Importance of Proton-Coupled Electron Transfer in Cathodic Regeneration of Organic Hydrides. *Chem. Commun.* **2019**, *55*, 5583−5586.[4] *This study explores proton-couped electron transfer in the electrochemical reduction of conjugate hydride acceptors to the corresponding hydride donors. When the pK_a values of the relevant radical cations are appropriate, the proton-coupled mechanism is shown to lower the electrochemical potential.*

INTRODUCTION

The conversion of carbon dioxide to value-added chemicals (e.g., polycarbonates) and fuels (e.g., methanol) is of increasing scientific interest, driven by the need to slow down the climate change caused by human-induced carbon dioxide emissions.[5,6] Some of the target chemical transformations for CO_2 utilization require a relatively small energy input and generally do not change the oxidation state of the carbon center. One such transformation involves the production of urea from CO_2 and NH_3, a mature technology currently used to produce 155 Mt/year of urea for agricultural fertilizers and other products.[7] However, urea production would need to increase ∼200-fold to compensate for the current anthropogenic carbon input. In contrast, the reductive transformations that generate carbon in lower oxidation states, such as +2 (formic acid), 0 (formaldehyde), and −2 (methanol), are more energy-intensive and challenging. The products obtained from these transformations can serve as fuels to generate electricity or heat. The reductive CO_2 conversion can be achieved chemically via thermal hydrogenation or electrochemically/photochemically by using water as a terminal proton and electron source. Although thermal methods are at a higher technology readiness level, with several methanol-producing plants via CO_2 hydrogenation currently in operation,[8] the electrochemical and photochemical methods

https://doi.org/10.1021/acs.accounts.1c00708
Acc. Chem. Res. 2022, 55, 844−856

are more advantageous because they are more readily coupled to renewable sources of energy, such as solar and wind. Furthermore, the theoretical thermal efficiencies of electrochemical methods are higher (can reach unity for an ideal cell) than those achievable by thermal methods (the ideal efficiency can be up to $1 - T_C/T_H$, where T_C is the absolute temperature of the cold reservoir and T_H is the absolute temperature of the hot reservoir, as known from the Carnot cycle). The losses in thermal processes are associated with the incompleteness of any heat-transfer process that occurs at temperatures that are not absolute zero. The electrochemical methods rely on charge-transfer processes, where all of the energy of an electron can be used up if resistance losses and overpotentials are negligible.[9]

Extensive mechanistic studies have been performed on transition-metal-based molecular electrocatalysts for CO_2 reduction, providing information regarding the factors that control catalytic rates, overpotentials, and product selectivity.[10−12] In general, the catalytic cycle is initiated by the metal-centered reduction, which is often coupled with the loss of a labile ligand (Scheme 1a). The reduced transition-metal complex becomes sufficiently nucleophilic to react either with CO_2 to form the metal carboxylate intermediate or with protons to form the metal hydride. The relative rates of these two reactions dictate the product selectivity: metal carboxylate intermediates lead to the reduction of carbon dioxide to CO and C_{2+} products, and metal hydride intermediates direct the reactivity toward proton-reduction and hydride-transfer products, such as formate and methanol. Careful control of thermodynamic parameters, such as the pK_a value of the proton donor, can be used to steer the reactivity in the desired direction.[13] The metal carboxylate intermediate M−CO_2 is usually a precursor for CO formation, and its M−OCO isomer is responsible for the formation of oxalate and beyond products.[14] The selective stabilization of one of the two carboxylate and hydride intermediates can be achieved using a proper choice of the metal−ligand couple.[10,15] Overall, homogeneous transition-metal-based catalysts often catalyze the reduction of CO_2 to CO,[16−22] less frequently the reduction to formate,[13,23−28] and very rarely the reduction to methanol.[29,30] Although more recent reports show how you can thermodynamically navigate toward formate formation,[23,26,31,32] there is still a need for the discovery of new catalysts that are more efficient at suppressing the hydrogen evolution reaction.

In natural photosynthesis, plants and other organisms convert CO_2 to energetically dense molecules using sunlight as an energy input. This process depends on a variety of cofactors, including nicotinamide adenine dinucleotide phosphate (NADPH), which is responsible for the reduction of "captured" CO_2 via a hydride-transfer (HT) mechanism (Scheme 1b). Specifically, CO_2 is captured within the Calvin cycle to generate 1,3-bisphosphoglycerate, which is then reduced via HT from NADPH to generate glyceraldehyde-3-phosphate, a key precursor in the self-synthesis of biomass and other energy-dense molecules (glucose).[33] The oxidized $NADP^+$ cofactor is then reduced back to the hydride form using sunlight as an energy source and water as an electron/proton source. Thus, the overall photocatalytic transformation is achieved by an organic reduction catalyst, NADPH. Photosynthesis demonstrates that plants can selectively synthesize the molecules necessary for their growth using the resources available to them, such as ambient CO_2, which comprises ∼0.04% of our atmospheric gases,[34] and earth-abundant CO_2 reduction organocatalysts.

Herein, we present our exploration of biomimetic NAPDH analogs as potential electro- and photocatalysts for the selective reduction of CO_2 to formate. Our work is motivated by the scalability and low cost of such earth-abundant organocatalytic systems. Furthermore, the HT mechanism is critical for the selective formation of formate, a product that is rarely formed when metal-based catalysts are used, thus avoiding the formation of CO. The overall catalytic cycle under investigation is shown in Scheme 1 and is divided into the HT and hydride regeneration steps. We first present the results of our work involving the HT step by discussing the thermodynamic hydricities of a series of carbon-based hydride donors (R−H) and their reactivity with CO_2. These studies provide insights into structure−property relationships that control the hydricities of R−H derivatives as well as kinetic barriers associated with the HT process. The second section of this report reviews our hydride regeneration approaches. We show how the proton-coupled electron-transfer (PCET) mechanism can be utilized to lower the overpotential for the electrochemical reduction of R^+ derivatives and to prevent the undesired dimerization of the one-electron-reduced $R^\bullet$ radical. We also show our studies of the photochemical regeneration of R−H derivatives using wide and midgap inorganic semiconductor photoelectrodes. Overall, our work provides important proof-of-principle demonstrations of successful metal-free (photo)electrocatalysis involving R−H donors. Furthermore, our work points out the challenges that still need to be addressed to enable fast and energy-efficient CO_2 reduction catalysis by NADPH analogs.

HYDRIDE TRANSFER TO CO_2

Thermodynamics

Metal-free hydrides, just like metal-based analogs, differ in their hydride donor ability based on their structural and electronic characteristics. To establish design strategies that contribute to stronger hydrides, thermodynamic parameters that describe their hydride donor ability need to be considered. For that purpose, the most readily applicable descriptor with the largest available database is thermodynamic hydricity (ΔG_{H^-}), defined as the standard Gibbs free energy required for hydride ion release:

$$R{-}H \rightarrow R^+ + H^- \quad (1)$$

Given that a high-energy intermediate, the hydride ion, is released, reaction 1 is never spontaneous and ΔG_{H^-} values are always positive numbers. A lower ΔG_{H^-} value indicates a stronger hydride (for example, ΔG_{H^-} for $LiAlH_4$ is 43 kcal/mol in acetonitrile[35]), and a higher ΔG_{H^-} value indicates weaker hydride donors (for example, ΔG_{H^-} for $NaBH_4$ is 50 kcal/mol in acetonitrile[35]). The ΔG_{H^-} values serve as excellent markers for the donor's HT abilities, decoupled from the nature of the hydride acceptor.

Despite many experimental hydricities reported for metal-based hydrides,[23,24,36−42] only a handful of stronger metal-free hydrides have been experimentally evaluated.[43−46] This trend is not consistent with experimental challenges associated with metal-based hydride donors: interactions of solvent and anion molecules with the metal-based conjugate hydride acceptor are known to affect the observed hydricities.[47,48] Such interactions do not affect metal-free hydride donors, making them easier to

https://doi.org/10.1021/acs.accounts.1c00708
Acc. Chem. Res. 2022, 55, 844−856

Scheme 2. Thermochemical Cycles Used to Experimentally Determine the ΔG_{H^-} Values

"potential-pK_a" method

$$RH \rightarrow R^- + H^+ \qquad \Delta G = 1.364\ \mathrm{p}K_a^{RH} \qquad (2a)$$
$$R^- \rightarrow R^{\cdot} + e^- \qquad \Delta G = 23.06\ E^0_{R^{\cdot}/R^-} \qquad (2b)$$
$$R^{\cdot} \rightarrow R^+ + e^- \qquad \Delta G = 23.06\ E^0_{R^+/R^{\cdot}} \qquad (2c)$$
$$H^+ + 2e^- \rightarrow H^- \qquad \Delta G^{H^+/H^-}_{DMSO/ACN} \qquad (2d)$$
$$RH \rightarrow R^+ + H^- \qquad \Delta G_{H^-}(RH) \qquad (2e)$$

"hydride transfer" method

$$RH + A^+ \rightarrow R^+ + AH \qquad \Delta G = -1.364\ log(K_{eq}) \qquad (3a)$$
$$AH \rightarrow AH + H^- \qquad \Delta G_{H^-}(AH) \qquad (3b)$$
$$RH \rightarrow R^+ + H^- \qquad \Delta G_{H^-}(RH) \qquad (3c)$$

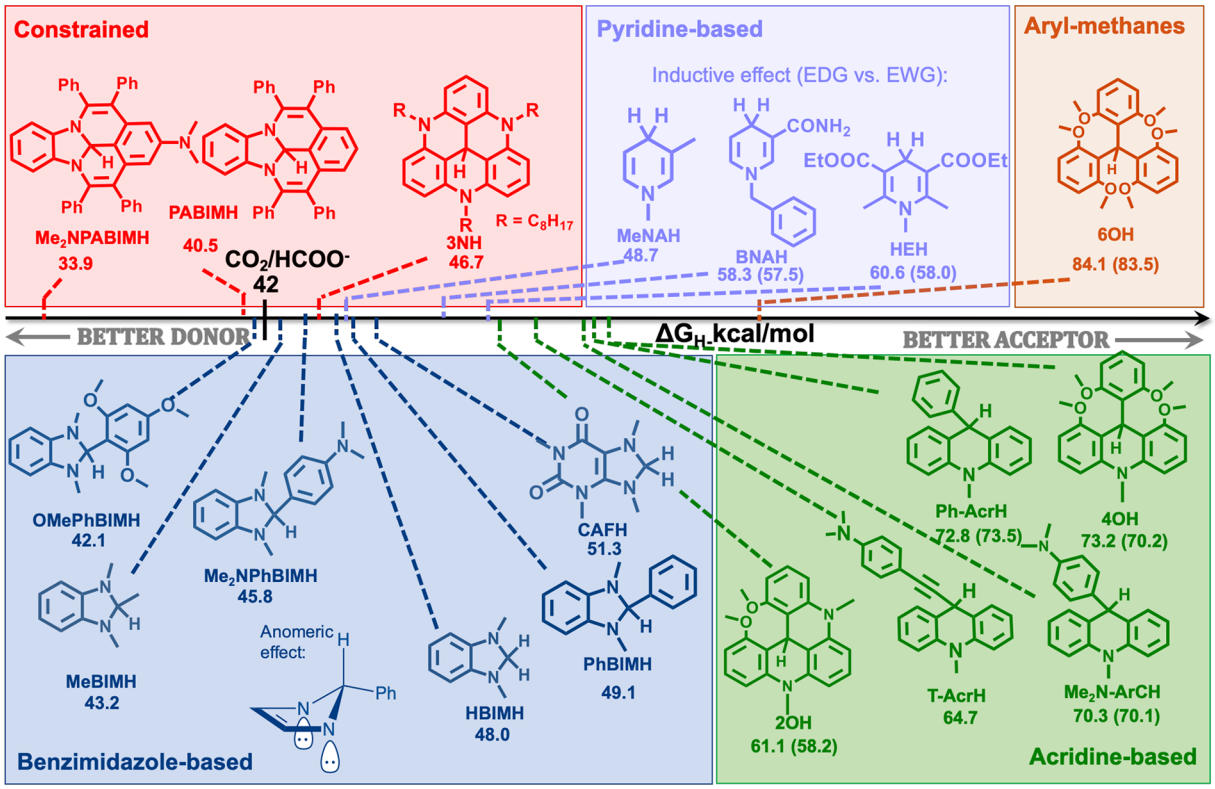

Figure 1. Calculated and experimental (in parentheses) thermodynamic hydricities for selected hydrides in DMSO. Data are taken from refs 1, 3, and 36.

study. Our group and others have utilized commonly used potential-pK_a and hydride-transfer methods, both based on thermochemical cycles,[23] to determine the ΔG_{H^-} values of metal-free hydride donors (Scheme 2). The potential-pK_a method utilizes a thermodynamic cycle that involves eqs 2a–d. In this approach, the ΔG values for eqs 2a–c are obtained from the pK_a values of R–H derivatives (using spectrophotometric titration), the experimentally obtained standard reduction potentials for $R^+/R^{\bullet}$ and $R^{\bullet}/R^-$ couples (using cyclic voltammetry), and the pK_a values of R–H derivatives (using spectrophotometric titration). The ΔG value for eq 2d is obtained from the standard reduction potential for the H^+/H^- couple. Given that this reduction potential is not directly available in nonaqueous solvents, several assumptions (mostly regarding solvation) were employed to derive the $\Delta G_{H^+/H^-}$ values of 69.9 and 54.7 kcal/mol in DMSO and ACN, respectively.[49] The potential-pK_a method has been utilized to obtain thermodynamic hydricities of weak hydrides, and the thermodynamic hydricity of stronger hydrides is more commonly determined using the hydride-transfer method (eqs 3a,b). In this method, the ΔG_{H^-} values are derived from ΔG_{HT} (eq 3a), obtained from the equilibrium constant for HT between a donor of interest R–H and a reference hydride acceptor A^+ with a known hydride affinity (expressed as the negative of the hydricity of A–H, eq 3b) and hydricity (ΔG_{HT}(AH)). For ΔG_{HT} to be experimentally measurable, the difference in hydricity between R–H and A–H needs to be in the ±2 to 3 kcal/mol range. As such, the method may require several hydride acceptors A^+ to be tested before the appropriate reference is established. It is experimentally less challenging to determine the enthalpic hydricity ΔH_{H^-} by measuring the heat change for the hydride-transfer reaction via calorimetry. However, the corresponding entropic contributions need to be negligible or consistent in order to use ΔH_{H^-} values to characterize a wide range of hydrides. Because this is not the case,[50] the ΔH_{H^-} values can be used only to compare structurally similar hydride donors.

Given the challenges associated with the experimental ΔG_{H^-} determination,[50] computational evaluation represents a more straightforward and easier alternative. The computational approach involves calculations of absolute Gibbs free energies for solvated species in eq 1. Although G_{R-H} and G_{R^+} can be accurately calculated with commonly used implicit solvent models, the computational treatment of the solvated H^- ion is far less trivial. Namely, the available solvation models fail to account for the interactions between the solvated hydride ion

https://doi.org/10.1021/acs.accounts.1c00708
Acc. Chem. Res. 2022, 55, 844–856

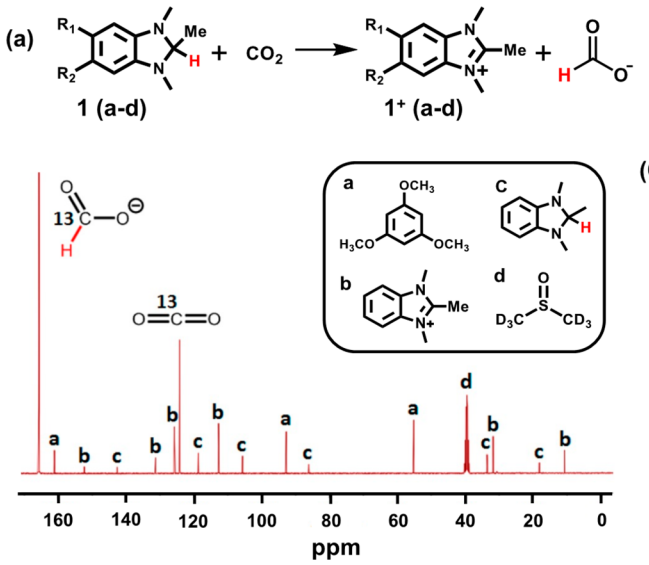

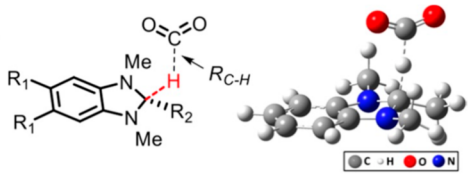

Hydride Donor	Formate Yield (%)	$\Delta G^{\ddagger}_{HT}$(298 K) (kcal/mol)	ΔG^{0}_{rxn}(298 K) (kcal/mol)	$R_{C\text{-}H}$(Å)
1a (R_1 = H, R_2 = H)	5	23.1	4.2	1.37
1b (R_1 = Me, R_2 = H)	4	22.1	2.0	1.39
1c (R_1 = H, R_2 = Me)	59 (66)	20.6	0.7	1.38
1d (R_1 = Me, R_2 = Me)	51	21.1	-1.7	1.39

Figure 2. Reduction of CO_2 to formate using organic hydrides: (a) ^{13}C NMR spectra of the reaction between MeBIMH and $^{13}CO_2$ in DMSO-d_6. (b) HT transition-state structure calculated at the RM06/6-31+G(d,p) level of theory. (c) Calculated ΔG^{o}_{HT} and $\Delta G^{\ddagger}_{HT}$ values for HT, along with the calculated C−H bond lengths in the transition state. Reproduced with permission from ref 2. Copyright 2019 American Chemical Society.

and solvent molecules, such as dispersion, repulsion, and hydrogen bonding. Instead, the calculation of absolute Gibbs free energies for the solvated hydride ion can be successfully circumvented by using the linear scaling approach, where G_H is extracted from the correlation between the experimental hydricity values and calculated G_{R-H} and G_{R^+} (eq 1).[50] Alternatively, the solvated G_{H^-} can be obtained from the calculation of G_{H^-} in the gas phase by adding the experimental correction for solvation effects.[1,50] Our previous studies indicated that the calculated hydricity values are in an reasonably good agreement with the experimental results (within 3 kcal/mol),[1,50] which enables screening of a wide range of metal-free hydride donors, even those that have yet to be synthesized.

For the HT reaction between hydride donor R−H and acceptor A^+ to take place spontaneously, the donor needs to have a lower ΔG_{H^-} value than the hydricity of the conjugate acceptor A−H. For example, Figure 1 compares ΔG_{H^-} values of metal-free hydride donors investigated in our laboratory, along with the hydricity of the formate ion. As shown, the reduction of CO_2 to formate is challenging and requires strong R−H donors with hydricities that are lower than 42.0 kcal/mol. Two structural arguments that contribute to stronger hydrides are (i) the ability to stabilize the positive charge formed on R^+ species after HT and (ii) the factors that lead to the relative destabilization of the donor R−H. In metal-free systems, the positive charge is stabilized through either extended delocalization or aromatization mechanisms. Aromatization upon HT is an efficient method to stabilize the positive charge formed and yields relatively strong hydrides. In fact, aromatization is the main driving force for hydride release from many biologically relevant cofactors, such as NADH,[52,53] $FADH_2$,[53] and H4MPT.[50,54] The positive charge on R^+ can be further stabilized through the inductive effect, achieved in the presence of electron-donating groups (such as amines, alcohols, etc.). For example, Figure 1 shows that ΔG_{H^-} values decrease in the HEH > BNAH > MeNAH series, illustrating the effect of increasing inductance with increasingly donating groups.

The relative destabilization of R−H also leads to improved hydricities. For example, the weakening of the R−H bond through the so-called anomeric effect[55,56] has been used to explain the lower ΔG_{H^-} values of benzimidazole-based derivatives (X−BIMH, Figure 1). Here, the hyperconjugation involving the donation of the lone pairs of electrons from the neighboring nitrogen atoms into the σ^* orbital of the C−H bond leads to the weakening of the C−H bond and thus the improved hydride-donating ability of R−H. In addition, hydride R−H can be destabilized via significant structural strain, where hydride ion removal results in a release of strain. Such behavior is exemplified by compounds 3NH, PABIMH, and Me_2NPABIMH, where the extended conjugation imposes a tendency of the molecule to adopt a planar conformation, imposing strain onto the sp^3-hybridized hydridic C−H bond in the compound. Combined, these electronic and structural factors can tune the thermodynamic hydricities of carbon-based hydride donors within the 30−90 kcal/mol range, enabling applications in many HT processes. Hydrides in Figure 1 can be classified into three structural groups with characteristic hydride donor abilities. First, arylmethanes are relatively weak hydrides (ΔG_{H^-} = 75−90 kcal/mol) and are not relevant to CO_2 reduction. Next, pyridine- and acridine-based hydrides display a significantly improved hydride donor ability (46−76 kcal/mol), which is achieved via R^+ aromatization upon hydride loss. These hydrides have already been employed in synthetic transformations as stoichiometric reducing reagents.[57−63] Strong hydride donors (with ΔG_{H^-} < 40 kcal/mol) are the most applicable for HT to CO_2, and the reactivities of these derivatives with CO_2 have been further explored.

Given that the hydricities of benzimidazoles are similar or even lower than that of formate (ΔG_{H^-} = 42 kcal/mol), these hydrides represent suitable candidates for CO_2 reduction reactions. Indeed, the benzimidazoles in Figure 2 were the first carbon-based hydrides reported to selectively reduce CO_2 to formate.[2] The experimentally observed reactivity correlates with the calculated free energies for HT, ΔG_{HT} (Figure 2). The highest formate yield (66%, Figure 2) was achieved using

https://doi.org/10.1021/acs.accounts.1c00708
Acc. Chem. Res. 2022, 55, 844−856

MeBIMH in the presence of KBF_4 in DMSO under mild conditions. The addition of exogenous salts stabilizes charged products, such as R^+ and $HCOO^-$, by increasing the ionic strength of the medium. Similarly, the HT reaction was found to be solvent-dependent, where more polar solvents resulted in higher yields as a result of the same effect on product stabilization. This study served as a proof of principle that selective CO_2 reduction can be carried out using carbon-based hydride donors.

The HT reactivity could certainly be further improved by using stronger hydride donors. However, as is always the case in catalysis, the improved reactivity of R−H would come at the expense of an increase in energy needed to regenerate the reduced form of the catalyst from R^+. This correlation is best observed in Figure 3, which plots the ΔG_{H^-} values of R−H as a

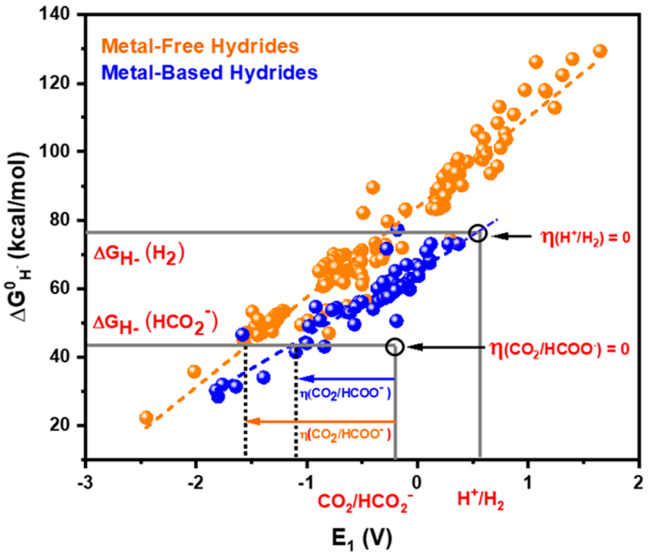

Figure 3. Scaling relationship between the thermodynamic hydricity ΔG_{H-} and the first electron reduction potential E_1 (vs NHE) of R^+ for metal-free (orange) and metal-based hydrides (blue) in acetonitrile. The dashed lines indicate the estimated overpotential for CO_2 reduction catalysis. Reproduced with permission from ref 50. Copyright 2018 Royal Society of Chemistry.

function of the standard reduction potential for the $R^+/R^\bullet$ couple.[50] The presence of a linear dependence is a clear indication that a scaling relationship exists between the two parameters, making it difficult to improve HT reactivity without introducing an overpotential in the catalyst regeneration step. Figure 3 also shows a point where an ideal catalyst for the reduction of CO_2 to formate should be, based on the standard reduction potential for the $CO_2/HCOO^-$ couple (−0.23 V vs NHE) and the hydricity of formate (42 kcal/mol). It is obvious from Figure 3 that none of the metal-free derivatives R−H exhibit the desired hydricity/reduction potential values and that a significant overpotential is expected in metal-free CO_2 reduction to formate (∼1.5 V). Similarly, a metal-based hydride donor exhibits a scaling relationship between ΔG_{H^-} and $E^o(M^{n+}/M^{(n-1)+})$ values, albeit with smaller overpotentials due to the lower bond-dissociation energy of the M−H bond.[50]

Kinetics

To further explore the origins of the sluggish reactivity observed in Figure 2, we investigated the HT kinetics from a series of organic hydrides to CO_2.[3] Several experimental conditions were explored to maximize formate production via CO_2 reduction by organohydrides. Namely, the highest formate yield (70%) was achieved at 100 °C, at a mild CO_2 pressure of ∼2.2 atm and in the presence of 20 equiv of KBF_4 in DMSO. Temperature-dependent studies were performed using the optimized reaction conditions in the temperature range of 70−100 °C for the reaction. The HT reactions were monitored using ^1H NMR spectroscopy (Figure 4a), and the observed changes in the reactant/product concentrations were modeled using kinetic equations derived from rate laws for two possible HT reactions (Figure 4b,c) at several temperatures (Figure 4c) to determine free-energy barriers ($\Delta G^{\ddagger}$) for

$$RH + CO_2 \rightarrow R^+ + HCOO^- \quad (4)$$

The experimental free-energy barrier for the HT to CO_2 was found to be in the range of $\Delta G^{\ddagger}$ = 15−21 kcal/mol for the reactions with thermodynamic driving forces in the range of ΔG_{rxn}= −11− 5 kcal/mol.

The Marcus formalism was applied to explore the correlation between the free-energy barrier ($\Delta G^{\ddagger}$) and the thermodynamic driving force (ΔG^o) for HT to CO_2. The goal of this study was to evaluate the reorganization energy associated with HT to CO_2. According to Marcus theory, the activation free energy barrier can be expressed as

$$\Delta G^{\ddagger} = W_r + \frac{\lambda}{4} + \frac{\Delta G^{0\prime}}{2} + \frac{(\Delta G^{0\prime})^2}{4\lambda} \quad (5)$$

where W_r is the free energy required for the formation of the precursor complex and ($\Delta G^{o\prime}$) is the thermodynamic driving force of the reaction, corrected for the free energy of the encounter complex. The reorganization energy λ is the energy associated with the reorganization of the nuclei and the solvent upon hydride transfer and is assumed to be independent of the structure of the hydride donor. The experimental value was found to be λ = 74 kcal/mol and was consistent with the value of λ = 70 kcal/mol obtained using DFT calculations. This reorganization energy was further partitioned into contributions from the hydride donor, RH, and from the hydride acceptor, CO_2, using the corresponding self-exchange reorganization energies λ_{RH} and λ_{CO_2} as follows:

$$\lambda = \frac{\lambda_{RH} + \lambda_{CO_2}}{2} \quad (6)$$

$$RH + R^+ \rightarrow R^+ + RH \quad \lambda_{RH}$$

$$HCOO^- + CO_2 \rightarrow CO_2 + HCOO^- \quad \lambda_{CO_2}$$

Self-exchange reorganization energies obtained using this approach were found to be quite high: λ_{RH} = 98 kcal/mol and λ_{CO_2} = 49 kcal/mol. The large λ_{CO_2} = 49 kcal/mol is most likely associated with the significant structural distortion associated with the conversion of the linear reactant, CO_2, to the bent formate ion. Similar arguments were used to explain the large self-exchange reorganization energy associated with the electron transfer to CO_2 to form the $CO_2^{\bullet-}$ radical anion.[64] The large λ_{RH} value shows that organic hydrides undergo significant structural rearrangement upon HT, and this reorganization is likely associated with the planarization of R^+.

To illustrate what these self-exchange values mean for the catalytic HT, we evaluated HT rates for a hypothetical electrocatalyst for CO_2 reduction to formate that operates via

https://doi.org/10.1021/acs.accounts.1c00708
Acc. Chem. Res. 2022, 55, 844−856

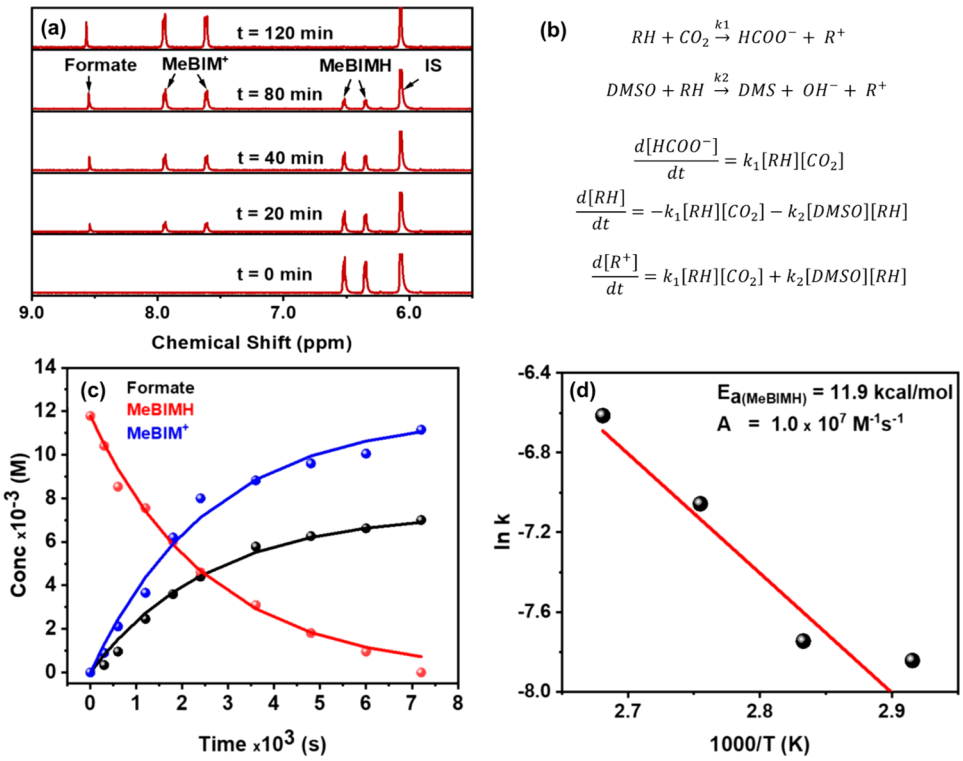

Figure 4. Kinetic studies of the HT reaction from MeBIMH to CO_2 in DMSO-d_6: (a) time-dependent ^{1}H NMR spectral characterization for the reaction of MeBIMH and CO_2; (b) two possible hydride-transfer reactions to CO_2 and solvent (DMSO); (c) change in the concentrations of reactants and products as a function of time for the HT (solid lines represent fits of the kinetic model); and (d) Arrhenius plot for the HT reaction obtained from temperature-dependent kinetic experiments. Reproduced with permission from ref 3. Copyright 2021 American Chemical Society.

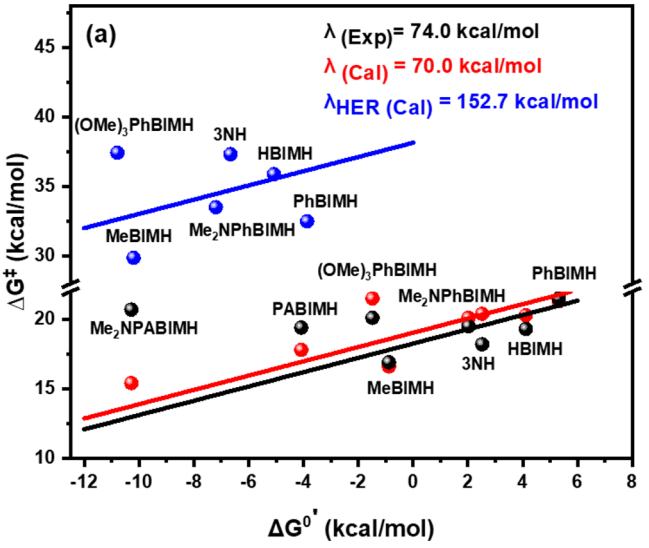

Figure 5. Correlation between free-energy barriers ($\Delta G^{\ddagger}$) and reaction free energies ($\Delta G^{0\prime}$) for HT between organic hydrides and CO_2 in DMSO at 100 °C. Experimental values are denoted by black circles, and calculated values are shown with red circles. Blue circles represent calculated values for HT to water (HER). Solid lines correspond to fits to the Marcus model. Reproduced with permission from ref 3. Copyright 2021 American Chemical Society.

outer-sphere hydride transfer in the DMSO solvent at room temperature and at the driving force of −0.1 eV (Table 1). Under these conditions, we found that the HT from organic hydride donor catalysts to CO_2 would occur at a rate of 2.5 × 10^{-6} M^{-1} s^{-1}, which is prohibitively slow. If organic hydride donor catalysts were replaced with metal-based hydride donors such as $[Ru(trpy)(bpy)H]^+$, then the HT rate would improve significantly to 8 × 10^{-3} M^{-1} s^{-1}. This finding shows that the metal-based hydride donors are expected to be kinetically much more efficient than the corresponding organic analogs. However, even with metal-based catalysts, the HT reaction is still quite slow, which explains why formate formation is less commonly observed as a product during homogeneous CO_2 reduction electrocatalysis. Our analysis also predicts the maximum rate for HT to CO_2, which involves a hypothetical hydride donor with self-exchange reorganization energy λ_{RH} = 0 kcal/mol. The value of 3 × 10^3 M^{-1} s^{-1} is many orders of magnitude better than that obtained for metal-free and metal-based hydrides. However, this is still barely sufficient to enable catalytic rates greater than 100 turnovers per second, which is required to keep up with the photon flux of solar irradiance. Nonetheless, it should be emphasized that the kinetic analysis shown here applies to systems that exclusively undergo outer-sphere hydride transfers and reactions in the DMSO solvent.

Table 1. Summary of Self-Exchange Reorganization Energies and Estimated HT Rate Constants for a Metal-Free, Metal-Based, and Ideal Hydride Donor for CO_2 Reduction that Operates at 25 °C with a −0.1 eV Thermodynamic Driving Force in the DMSO Solvent[a]

hydride donor	λ_{RH} (kcal/mol)	λ (kcal/mol)	k_{HT} (M^{-1} s^{-1})
NADH analogue	98.4	74.0	2.5 × 10^{-6}
$[Ru(trpy)(bby)H]^+$	60.0	54.6	8.0 × 10^{-3}
ideal	0	24.6	3.0 × 10^{-3}

[a]Reproduced with permission from ref 3. Copyright 2021 American Chemical Society.

https://doi.org/10.1021/acs.accounts.1c00708
Acc. Chem. Res. 2022, 55, 844−856

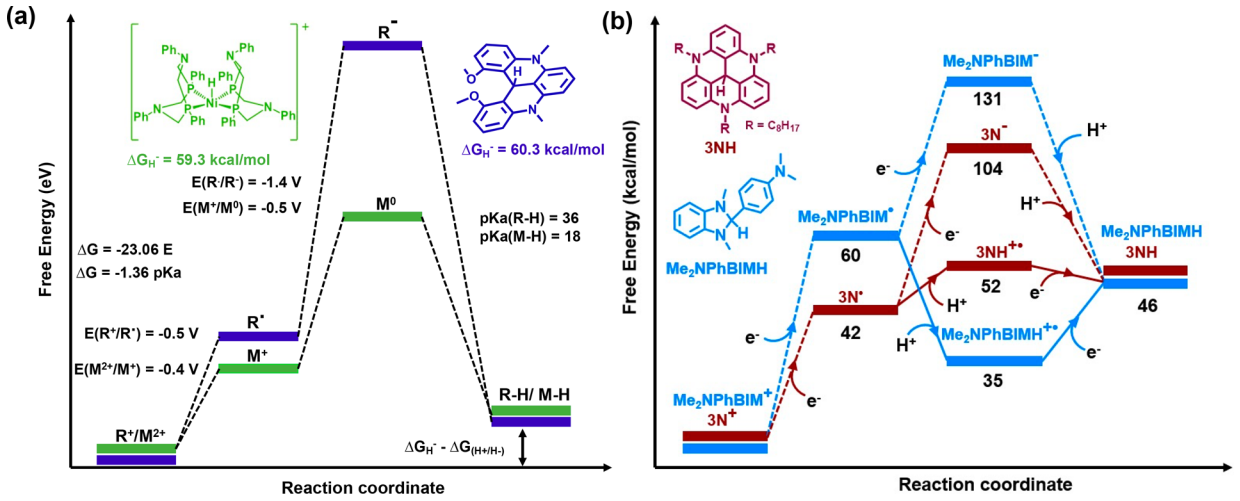

Figure 6. Comparison of the energy diagram profiles for (a) the regeneration of a metal-based hydride (($[Ni(P^{Ph}{}_2N^{Ph})_2H]^+$) (green color) and a metal-free hydride (2OH) (blue color) in acetonitrile and (b) the regeneration via electron−electron−proton (dotted line) and electron−proton−electron sequences (solid line) for benzimidazole-based (blue) and acridine-based hydrides (brown) in DMSO. Reproduced with permission from refs 1 and 4. Copyrights 2018 American Chemical Society and 2019 Royal Society of Chemistry.

Other mechanisms, such as CO_2 insertion into the hydride bond,[65] and different solvent systems may contribute to higher catalytic activities, as witnessed by reports on several CO_2-to-formate metal-based catalysts.

HYDRIDE REGENERATION

Electrochemical Regeneration

Organic hydride donors have been extensively used as stoichiometric reducing reagents in many organic HT transformations. However, their use as catalysts has been limited by the difficulties associated with hydride regeneration. First, the electrochemical regeneration of organic hydrides from R^+ derivatives is hampered by the tendency of one-electron-reduced $R^\bullet$ radicals to dimerize.[4,52,66] The dimer formation is irreversible, leading to the deactivation of the catalyst. We found that the dimerization rate can be reduced by the introduction of bulky substituents. For example, functionalization at the 2-position of benzimidazolium derivatives with bulky substituents, such as a mesityl group or a (1,3,5)-trimethoxybenzene group, stabilized the radical form. This was evidenced by their CV, which illustrated a reversible couple for the first reduction of the BIM^+ derivatives.[4] In addition, the functionalization at the 2-position also imparted an additional driving force to HT from BIMH due to additional R^+ stabilization, relative to the unfunctionalized HBIMH.[3]

The second challenge is associated with exceptionally negative standard reduction potentials for the $R^\bullet/R^-$ couple. To exemplify this, Figure 6 compares the regeneration-energy landscape for one of our organic hydride, 2OH, with the corresponding energy landscape for the Ni-based hydride donor that exhibits essentially identical hydricity. The first reduction steps, namely, $R^+/R^\bullet$ for the organic analog and the Ni^{2+}/Ni^+ couple for the metal-based derivative, occur with similar standard reduction potentials (∼−0.5 V vs NHE). However, the energy requirements for the second reduction step ($R^\bullet/R^-$ and Ni^+/Ni^0) are significantly different: organic hydrides require a potential of −1.4 V vs NHE, but the metal-based system undergoes a second reduction step at only −0.5 V vs NHE. Such differences in the energy landscapes clearly point to the ability of d orbitals on metal centers to accumulate multiple charges at relatively modest potentials, whereas metal-free p orbitals cannot screen the accumulated charges as efficiently. Thus, an efficient approach to the regeneration of metal-free hydrides must avoid the formation of high-energy R^- intermediates, which can in principle be achieved using PCET (Figure 6). Specifically, if the pK_a values of $RH^{\bullet+}$ and the proton source are selected to enable the protonation of $R^\bullet$, the subsequent reduction step involving the $RH^{\bullet+}/RH$ couple is expected to occur at more positive potentials. Such PCET mechanisms are often utilized in natural and artificial catalysis and are an excellent method for minimizing energy penalties associated with the formation of charged intermediates.

To pinpoint the conditions needed to perform PCET during the regeneration of our organic hydrides, we computationally evaluated the pK_a values of our $RH^{\bullet+}$ intermediates (Figure 7).[4] We found that the pK_a values of acridine-based hydrides

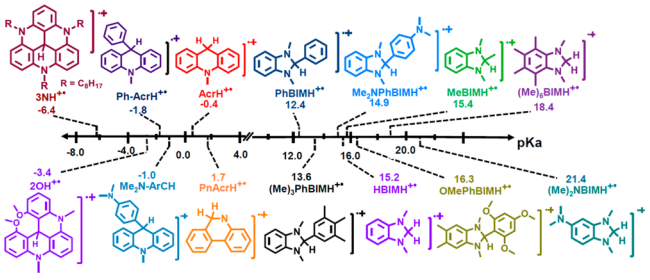

Figure 7. pK_a values for the radical cation forms of acridine and benzimidazole model compounds in DMSO. Values were obtained from DFT calculations at the wB97XD/6-311+G(d,p) level of theory. Data were taken from ref 4.

tend to be very low, in the range of −6.4 to +1.7 in DMSO. These values indicate that the PCET mechanism with acridine-based derivatives can operate only under extremely acidic conditions, which are impractical for electrocatalysis. However, the situation was different for benzimidazole-based derivates, where $pK_a(RH^{\bullet+})$ values are in the 12.4−21.4 range. Higher pK_a values of benzimidazole derivatives were explained by differences in the stability of neutral $R^\bullet$ radicals: cyclopentyl

https://doi.org/10.1021/acs.accounts.1c00708
Acc. Chem. Res. 2022, 55, 844−856

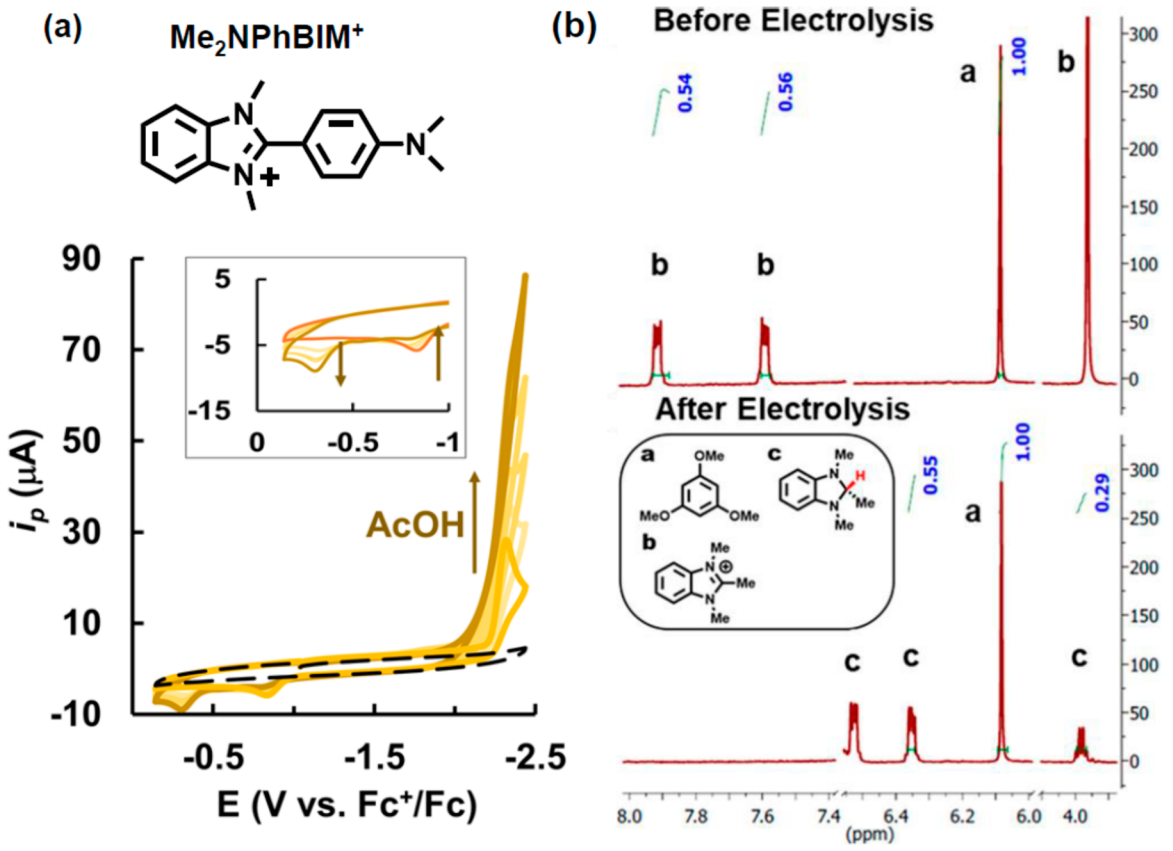

Figure 8. (a) Cyclic voltammograms of $Me_2NPhBIM^+$ in the presence of AcOH in DMSO. (b) ^1H NMR spectra of the catholyte solution before and after electrolysis in DMSO-d_6. Reproduced with permission from refs 4 and 2, respectively. Copyright 2019 Royal Society of Chemistry and 2019 American Chemical Society.

radicals in benzimidazoles are destabilized by the ring strain, even more so than the corresponding ring-strain destabilization associated with cyclohexyl radicals in acridines. These acidity constants indicate that the efficient protonation of benzimidazole-based $R^\bullet$ intermediates can be achieved under mild conditions using weak acids. Once protonated, $RH^{\bullet+}$ is easily reduced, with standard reduction potentials moving into the $E^o(RH^{\bullet+}/RH)$ = −0.34 to +0.19 V vs NHE range. Such a positive shift in the second reduction step changes the potential-liming process to the first reduction process associated with the $R^+/R^\bullet$ couple. Thus, the negative effects associated with the high-energy R^- intermediates can be efficiently circumvented in the case of benzimidazole-based hydrides.

The significance of these theoretical predictions was tested using the benzimidazole $Me_2NPhBIM^+$.[4] The cyclic voltammogram of $Me_2NPhBIM^+$ (Figure 8A) showed that the first reduction step, associated with the $R^+/R^\bullet$ couple, is chemically irreversible, and this behavior has been assigned to the radical dimerization process, which was confirmed by the appearance of the dimer oxidation peak at −0.84 V vs Fc/Fc^+ (−0.21 V vs NHE) in the return sweep. In the presence of acetic acid as a proton source, the dimerization process is suppressed, which can be observed as the disappearance of the dimer oxidation peak in the anodic sweep. Instead, the PCET mechanism takes place, leading to the formation of the hydride form, $Me_2NPhBIMH$, as evidenced by the appearance of the hydride oxidation peak at −0.34 V vs Fc/Fc^+ (+0.29 V vs NHE). The overall effect of the PCET mechanism is notable: it not only suppresses the unwanted radical dimerization process but also lowers the energy requirements for the hydride regeneration. We further demonstrated that the regeneration of benzimidazole hydrides can be achieved efficiently using controlled-potential electrolysis, where the NMR spectra of the catholyte before and after electrolysis illustrates the quantitative conversion from the cation to the hydride form (Figure 8B).

Photochemical Regeneration

Apart from the electrochemical regeneration, organic hydride donors can also be regenerated photochemically analogously to natural photosynthesis. In this approach, the light is absorbed by a semiconductor to generate electrons needed for the hydride formation. The photochemical approach of organic hydride donors is appealing because it combines the use of a renewable solar energy source with solar fuel production. In our previous work, we explored the photochemical regeneration of organic hydrides by placing the corresponding hydride acceptors R^+ in contact with p-type mid- and wide-gap inorganic semiconductors, GaP and NiO. In these studies, light harvesting was achieved either by the organic moiety (R^+ or $R^\bullet$) or by the semiconductor (GaP), and the regeneration mechanisms were explored using time-resolved laser spectroscopy. To avoid challenges associated with the dimerization of neutral radical $R^\bullet$ species, the photochemical studies were performed using organic hydride donors that produce stable radicals.

In our initial work, we explored light-induced electron transfer from p-GaP to physiosorbed triarylmethane, flavin, and acridine R^+ derivatives (Figure 9a). The R^+/GaP system represents a dual light-harvesting assembly: the blue photons

https://doi.org/10.1021/acs.accounts.1c00708
Acc. Chem. Res. 2022, 55, 844−856

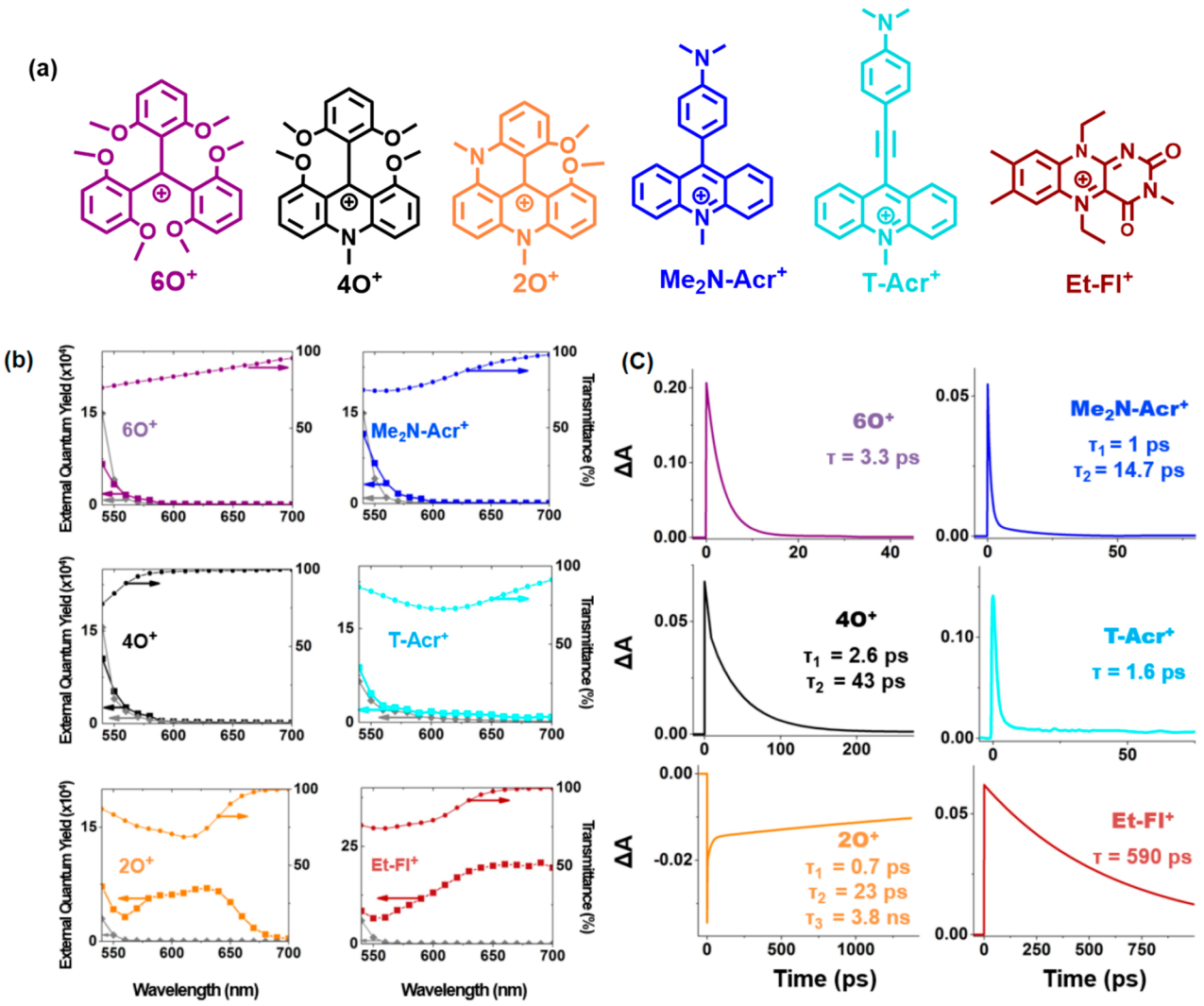

Figure 9. Photoreduction of the R^+/GaP dual absorber system: (a) structures of R^+; (b) photocurrent response measurements of p-GaP sensitized in the presence (colored squares) and absence (gray diamonds) of R^+ derivatives, where colored circles represent the transmittance of the corresponding R^+ derivatives in solution; and (c) kinetic transient absorption traces of model compounds in acetonitrile. Reproduced with permission from ref 67. Copyright 2016 American Chemical Society.

can be absorbed by GaP, and red photons can be absorbed by R^+. Thus, the R^+ derivatives were chosen on the basis of their ability to absorb light above 550 nm (absorption cutoff for p-GaP) and their capability to inject holes into p-GaP upon photoexcitation. Indeed, all dyes exhibited favorable thermodynamic characteristics for photoinduced electron transfer from p-GaP, as determined using their UV−vis absorption spectra and cyclic voltammograms.[67] The photochemical reduction of R^+ derivatives to the corresponding neutral $R^\bullet$ derivatives was achieved efficiently for the photoexcitation of GaP, as illustrated by the current increase at wavelengths shorter than 550 nm (Figure 9b). However, despite favorable thermodynamics, the photoelectrochemical measurements illustrated successful sub-band-gap sensitization for only $2O^+$ and Et-FI$^+$, as represented by the rise in photocurrent above 550 nm (Figure 9a). The lack of a subgap photocurrent in other dyes was explained by their short-lived excited-state lifetimes and confirmed by the detection of short-lived transients in pump−probe spectroscopy measurements of these dyes in solution (Figure 9c). Thus, the dual light-harvesting mechanism explored in this study works well if the excited-state lifetime of R^+ analogs exceeds several hundred picoseconds. Overall, this study illustrated that the first electron reduction of R^+ analogs can be efficiently achieved using photoactive p-type semiconductors.

In the follow-up study, we explored the dye-sensitization approach as a mechanism of performing the two-electron reduction of R^+ to enable the regeneration of organic hydride donors.[1,51] Unfortunately, complete regeneration could not be achieved using p-GaP because its valence-band edge energy does not provide sufficient driving force for the second electron reduction of most R^+ derivatives. To circumvent this challenge, we instead explored the use of a wide-gap semiconductor, p-NiO. The valence band energy of p-NiO enables hole injections from photoexcited R^+ and $R^\bullet$ radical species (Scheme 3b). Each photoreduction step was studied using femtosecond transient absorption on the synthesized $2O^+$@p-NiO and $2O^\bullet$@p-NiO composites. Although the obtained time-resolved data point toward the feasible photochemical conversion of $2O^+$ to the corresponding hydride 2OH with the multiple-electron accumulation approach, several drawbacks remain to be addressed. First, the $2O^+$@p-

https://doi.org/10.1021/acs.accounts.1c00708
Acc. Chem. Res. 2022, 55, 844−856

Scheme 3. (a) Schematic Representation of the Multielectron Accumulation Approach Used for the Photochemical Reduction of $2O^+$ to 2OH and (b) Energy Diagram Showing the Band Edge Potentials for NiO and Ground- and Excited-State Reduction Potentials of $2O^+$ and $2O^{\bullet}$[a]

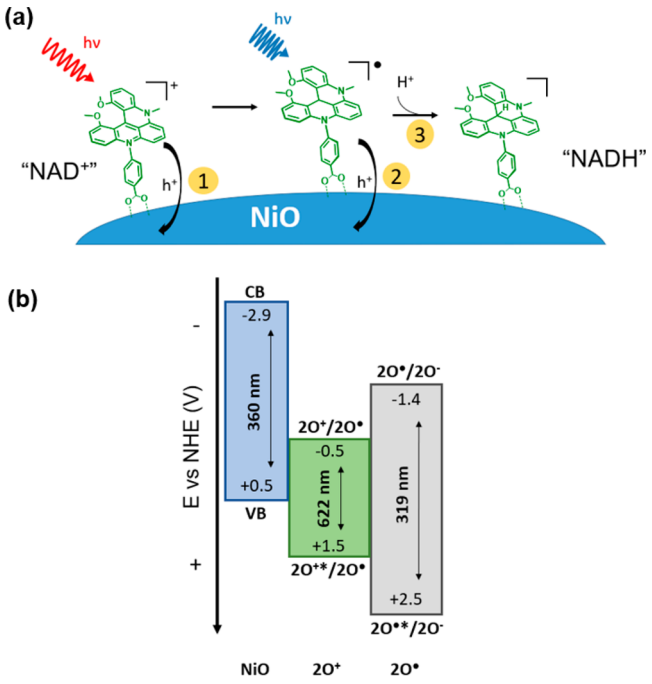

[a]Reproduced with permission from ref 51. Copyright 2019 American Chemical Society.

NiO composite exhibits rapid charge recombination: much of the charge-separated population recombines within 40 ps, caused in part by the poor electrical conductivity of p-NiO. Furthermore, the absorption of the $2O^{\bullet}$@p-NiO composite in the visible range is low, making it an inefficient harvester of solar radiation. Future studies should focus on the design of NAD^+ analogs that can achieve the long-distance charge separation and that can produce radicals with favorable absorption properties in the visible range.

CONCLUSIONS AND OUTLOOK

Our discoveries of the efficient hydride transfer to CO_2 and the successful regeneration of hydride donors using proton-coupled mechanisms represent important steps toward organocatalytic reduction processes. However, despite the tremendous effort and significant advances in recent years, several outstanding challenges need to be addressed before the metal-free catalytic system is realized. First, our studies indicate that the HT kinetics are sluggish. To enable room-temperature catalysis, hydride donors with low R−H/R^+ self-exchange reorganization energies need to be discovered. One possible way that this can be achieved is by minimizing the structural change that occurs as the hydride forms, where the sp^3 carbon center is converted to the cation form containing a planar sp^2 carbocation. The second challenge is associated with the large overpotential associated with the catalytic reduction of CO_2 to formate by organic (and metal-based) hydrides. Finding creative ways to circumvent the scaling relationships shown in Figure 3 will be essential for the discovery of fast and selective CO_2 reduction catalysts. An interesting method where this can be achieved has been put forward by Yang and coauthors,[26] who point out that HT in enzymatic CO_2/$HCOO^-$ conversion involves a bidirectional mechanism with electron- and proton-transfer steps occurring from separate moieties of the catalyst. The discovery of biomimetic catalysts with similar behavior can lead to efficient lowering of the reaction overpotential because the pK_a value of the proton source and the standard reduction potential of the electron source can be independently tuned to achieve ideal thermodynamic conditions for catalysis.

Once these challenges are addressed, metal-free HT catalysts are expected to serve as excellent alternatives for their metal-based counterparts. The most obvious advantages of using metal-free hydrides are that they are composed of earth-abundant elements and that they do not impose a threat to the environment. In addition, the CO_2 reduction by organic hydride donors proceeds with high selectively resulting from the HT mechanism: because none of the intermediates, R^+, $R^{\bullet}$, and R−H, exhibit appreciable binding interactions with CO_2, the formation of CO does not occur. This reactivity can be explored to enable the sequence of HT steps, starting with the reduction of CO_2 to formate, followed by the reduction of formate to formaldehyde and ending with the reduction of formaldehyde to methanol. Overall, this proton-coupled six-electron reduction of CO_2 to methanol, if catalyzed by inexpensive organocatalysts, represents an appealing approach to large-scale CO_2 upcycling using renewable energy sources.

AUTHOR INFORMATION

Corresponding Author

Ksenija D. Glusac − *Department of Chemistry, University of Illinois at Chicago, Chicago, Illinois 60607, United States; Chemical Sciences and Engineering Division, Argonne National Laboratory, Lemont, Illinois 60439, United States;* orcid.org/0000-0002-2734-057X; Email: glusac@uic.edu

Authors

Stefan Ilic − *Department of Chemistry, University of Illinois at Chicago, Chicago, Illinois 60607, United States; Chemical Sciences and Engineering Division, Argonne National Laboratory, Lemont, Illinois 60439, United States;* orcid.org/0000-0002-6305-4001

Jonathan L. Gesiorski − *Department of Chemistry, University of Illinois at Chicago, Chicago, Illinois 60607, United States*

Ravindra B. Weerasooriya − *Department of Chemistry, University of Illinois at Chicago, Chicago, Illinois 60607, United States; Chemical Sciences and Engineering Division, Argonne National Laboratory, Lemont, Illinois 60439, United States*

Complete contact information is available at: https://pubs.acs.org/10.1021/acs.accounts.1c00708

Notes

The authors declare no competing financial interest.

Biographies

Stefan Ilic obtained his Ph.D. at the University of Illinois Chicago in 2019 and then conducted his postdoctoral research at Virginia Tech, mentored by Prof. Amanda J. Morris. He is currently working at Argonne National Laboratory as a postdoctoral appointee in the

https://doi.org/10.1021/acs.accounts.1c00708
Acc. Chem. Res. 2022, 55, 844−856

JCESR hub. His research interests focus on clean energy conversion and storage systems.

Jonathan L. Gesiorski obtained his M.Sc. at the University of Illinois Chicago in 2021. His research in the Glusac group focused on biomimetic NADH analog catalysts.

Ravindra B. Weerasooriya obtained his Ph.D. at the University of Illinois Chicago in 2021. His research in the Glusac group focused on biomimetic NADH analog catalysts.

Ksenija D. Glusac obtained her Ph.D. at the University of Florida and then completed her postdoctoral training at Stanford University. She started her independent academic career at Bowling Green State University, where she spent 10 years. She is currently a professor of chemistry at the University of Illinois Chicago with a joint appointment at Argonne National Laboratory. Her research is focused on carbon-based motifs in photocatalysts and electrocatalysts relevant to energy storage and solar fuel applications.

■ ACKNOWLEDGMENTS

Ongoing research is supported by the National Science Foundation under award 1954298.

■ REFERENCES

(1) Ilic, S.; Pandey Kadel, U.; Basdogan, Y.; Keith, J. A.; Glusac, K. D. Thermodynamic Hydricities of Biomimetic Organic Hydride Donors. *J. Am. Chem. Soc.* **2018**, *140*, 4569−4579.
(2) Lim, C.-H.; Ilic, S.; Alherz, A.; Worrell, B. T.; Bacon, S. S.; Hynes, J. T.; Glusac, K. D.; Musgrave, C. B. Benzimidazoles as Metal-Free and Recyclable Hydrides for CO_2 Reduction to Formate. *J. Am. Chem. Soc.* **2019**, *141*, 272−280.
(3) Weerasooriya, R. B.; Gesiorski, J. L.; Alherz, A.; Ilic, S.; Hargenrader, G. N.; Musgrave, C. B.; Glusac, K. D. Kinetics of Hydride Transfer from Catalytic Metal-Free Hydride Donors to CO_2. *J. Phys. Chem. Lett.* **2021**, *12*, 2306−2311.
(4) Ilic, S.; Alherz, A.; Musgrave, C. B.; Glusac, K. D. Importance of Proton-Coupled Electron Transfer in Cathodic Regeneration of Organic Hydrides. *Chem. Commun.* **2019**, *55*, 5583−5586.
(5) Hepburn, C.; Adlen, E.; Beddington, J.; Carter, E. A.; Fuss, S.; Mac Dowell, N.; Minx, J. C.; Smith, P.; Williams, C. K. The Technological and Economic Prospects for CO_2 Utilization and Removal. *Nature* **2019**, *575*, 87−97.
(6) Aresta, M.; Dibenedetto, A.; Angelini, A. Catalysis for the Valorization of Exhaust Carbon: From CO_2 to Chemicals, Materials, and Fuels. Technological Use of CO_2. *Chem. Rev.* **2014**, *114*, 1709−1742.
(7) Parsons Brinckerhoff. *Accelerating the Uptake of CCS: Industrial Use of Captured Carbon Dioxide*; 2011.
(8) Peter, S. C. Reduction of CO_2 to Chemicals and Fuels: A Solution to Global Warming and Energy Crisis. *ACS Energy Letters* **2018**, *3*, 1557−1561.
(9) Hassanzadeh, H.; Mansouri, S. H. Efficiency of Ideal Fuel Cell and Carnot Cycle from a Fundamental Perspective. *Proceedings of the Institution of Mechanical Engineers, Part A: Journal of Power and Energy* **2005**, *219*, 245−254.
(10) Francke, R.; Schille, B.; Roemelt, M. Homogeneously Catalyzed Electroreduction of Carbon Dioxide—Methods, Mechanisms, and Catalysts. *Chem. Rev.* **2018**, *118*, 4631−4701.
(11) Elouarzaki, K.; Kannan, V.; Jose, V.; Sabharwal, H. S.; Lee, J.-M. Recent Trends, Benchmarking, and Challenges of Electrochemical Reduction of CO2 by Molecular Catalysts. *Adv. Energy Mater.* **2019**, *9*, 1900090.
(12) Costentin, C.; Robert, M.; Savéant, J.-M. Catalysis of the Electrochemical Reduction of Carbon Dioxide. *Chem. Soc. Rev.* **2013**, *42*, 2423−2436.
(13) Barlow, J. M.; Yang, J. Y. Thermodynamic Considerations for Optimizing Selective CO_2 Reduction by Molecular Catalysts. *ACS Central Science* **2019**, *5*, 580−588.
(14) Saouma, C. T.; Day, M. W.; Peters, J. C. CO_2 Reduction by Fe(I): Solvent Control of C−O Cleavage versus C−C Coupling. *Chemical Science* **2013**, *4*, 4042−4051.
(15) Savéant, J.-M. Molecular Catalysis of Electrochemical Reactions. Mechanistic Aspects. *Chem. Rev.* **2008**, *108*, 2348−2378.
(16) Elgrishi, N.; Chambers, M. B.; Artero, V.; Fontecave, M. Terpyridine Complexes of First Row Transition Metals and Electrochemical Reduction of CO_2 to CO. *Phys. Chem. Chem. Phys.* **2014**, *16*, 13635−13644.
(17) Elgrishi, N.; Chambers, M. B.; Fontecave, M. Turning It off! Disfavouring Hydrogen Evolution to Enhance Selectivity for CO Production during Homogeneous CO_2 Reduction by Cobalt−Terpyridine Complexes. *Chemical Science* **2015**, *6*, 2522−2531.
(18) Zhanaidarova, A.; Jones, S. C.; Despagnet-Ayoub, E.; Pimentel, B. R.; Kubiak, C. P. Re(tBu-bpy)$(CO)_3$Cl Supported on Multi-Walled Carbon Nanotubes Selectively Reduces CO_2 in Water. *J. Am. Chem. Soc.* **2019**, *141*, 17270−17277.
(19) Chen, Z.; Chen, C.; Weinberg, D. R.; Kang, P.; Concepcion, J. J.; Harrison, D. P.; Brookhart, M. S.; Meyer, T. J. Electrocatalytic Reduction of CO_2 to CO by Polypyridyl Ruthenium Complexes. *Chem. Commun.* **2011**, *47*, 12607−12609.
(20) Chen, Z.; Kang, P.; Zhang, M.-T.; Meyer, T. J. Making Syngas Electrocatalytically Using a Polypyridyl Ruthenium Catalyst. *Chem. Commun.* **2014**, *50*, 335−337.
(21) Woolerton, T. W.; Sheard, S.; Reisner, E.; Pierce, E.; Ragsdale, S. W.; Armstrong, F. A. Efficient and Clean Photoreduction of CO_2 to CO by Enzyme-Modified TiO_2 Nanoparticles Using Visible Light. *J. Am. Chem. Soc.* **2010**, *132*, 2132−2133.
(22) Kuehnel, M. F.; Orchard, K. L.; Dalle, K. E.; Reisner, E. Selective Photocatalytic CO_2 Reduction in Water through Anchoring of a Molecular Ni Catalyst on CdS Nanocrystals. *J. Am. Chem. Soc.* **2017**, *139*, 7217−7223.
(23) Wiedner, E. S.; Chambers, M. B.; Pitman, C. L.; Bullock, R. M.; Miller, A. J. M.; Appel, A. M. Thermodynamic Hydricity of Transition Metal Hydrides. *Chem. Rev.* **2016**, *116*, 8655−8692.
(24) Waldie, K. M.; Ostericher, A. L.; Reineke, M. H.; Sasayama, A. F.; Kubiak, C. P. Hydricity of Transition-Metal Hydrides: Thermodynamic Considerations for CO_2 Reduction. *ACS Catal.* **2018**, *8*, 1313−1324.
(25) Kinzel, N. W.; Werlé, C.; Leitner, W. Transition Metal Complexes as Catalysts for the Electroconversion of CO_2: An Organometallic Perspective. *Angew. Chem., Int. Ed.* **2021**, *60*, 11628−11686.
(26) Yang, J. Y.; Kerr, T. A.; Wang, X. S.; Barlow, J. M. Reducing CO_2 to HCO_2^- at Mild Potentials: Lessons from Formate Dehydrogenase. *J. Am. Chem. Soc.* **2020**, *142*, 19438−19445.
(27) Cunningham, D. W.; Barlow, J. M.; Velazquez, R. S.; Yang, J. Y. Reversible and Selective CO_2 to HCO_2^- Electrocatalysis near the Thermodynamic Potential. *Angew. Chem., Int. Ed.* **2020**, *59*, 4443−4447.
(28) Ceballos, B. M.; Yang, J. Y. Highly Selective Electrocatalytic CO_2 Reduction by $[Pt(dmpe)_2]^{2+}$ through Kinetic and Thermodynamic Control. *Organometallics* **2020**, *39*, 1491−1496.
(29) Boston, D. J.; Pachón, Y. M. F.; Lezna, R. O.; de Tacconi, N. R.; MacDonnell, F. M. Electrocatalytic and Photocatalytic Conversion of CO_2 to Methanol Using Ruthenium Complexes with Internal Pyridyl Cocatalysts. *Inorg. Chem.* **2014**, *53*, 6544−6553.
(30) Bi, J.; Hou, P.; Liu, F.-W.; Kang, P. Electrocatalytic Reduction of CO_2 to Methanol by Iron Tetradentate Phosphine Complex Through Amidation Strategy. *ChemSusChem* **2019**, *12*, 2195−2201.
(31) Taheri, A.; Thompson, E. J.; Fettinger, J. C.; Berben, L. A. An Iron Electrocatalyst for Selective Reduction of CO_2 to Formate in Water: Including Thermochemical Insights. *ACS Catal.* **2015**, *5*, 7140−7151.
(32) Bhattacharya, M.; Sebghati, S.; Vanderlinden, R. T.; Saouma, C. T. Toward Combined Carbon Capture and Recycling: Addition of an

https://doi.org/10.1021/acs.accounts.1c00708
Acc. Chem. Res. 2022, 55, 844−856

Amine Alters Product Selectivity from CO to Formic Acid in Manganese Catalyzed Reduction of CO_2. *J. Am. Chem. Soc.* **2020**, *142*, 17589−17597.
(33) Schneider, G.; Lindqvist, Y.; Branden, C. I. Rubisco: Structure and Mechanism. *Annu. Rev. Biophys. Biomol. Struct.* **1992**, *21*, 119−143.
(34) Olah, G. A.; Prakash, G. K. S.; Goeppert, A. Anthropogenic Chemical Carbon Cycle for a Sustainable Future. *J. Am. Chem. Soc.* **2011**, *133*, 12881−12898.
(35) Heiden, Z. M.; Lathem, A. P. Establishing the Hydride Donor Abilities of Main Group Hydrides. *Organometallics* **2015**, *34*, 1818−1827.
(36) Tsay, C.; Livesay, B. N.; Ruelas, S.; Yang, J. Y. Solvation Effects on Transition Metal Hydricity. *J. Am. Chem. Soc.* **2015**, *137*, 14114−14121.
(37) Curtis, C. J.; Miedaner, A.; Ellis, W. W.; DuBois, D. L. Measurement of the Hydride Donor Abilities of $[HM(diphosphine)_2]^+$ Complexes (M = Ni, Pt) by Heterolytic Activation of Hydrogen. *J. Am. Chem. Soc.* **2002**, *124*, 1918−1925.
(38) Raebiger, J. W.; Miedaner, A.; Curtis, C. J.; Miller, S. M.; Anderson, O. P.; DuBois, D. L. Using Ligand Bite Angles To Control the Hydricity of Palladium Diphosphine Complexes. *J. Am. Chem. Soc.* **2004**, *126*, 5502−5514.
(39) Creutz, C.; Chou, M. H. Hydricities of d^6 Metal Hydride Complexes in Water. *J. Am. Chem. Soc.* **2009**, *131*, 2794−2795.
(40) Matsubara, Y.; Fujita, E.; Doherty, M. D.; Muckerman, J. T.; Creutz, C. Thermodynamic and Kinetic Hydricity of Ruthenium(II) Hydride Complexes. *J. Am. Chem. Soc.* **2012**, *134*, 15743−15757.
(41) DuBois, D. L.; Berning, D. E. Hydricity of Transition-Metal Hydrides and Its Role in CO_2 Reduction. *Appl. Organomet. Chem.* **2000**, *14*, 860−862.
(42) Brereton, K. R.; Smith, N. E.; Hazari, N.; Miller, A. J. M. Thermodynamic and Kinetic Hydricity of Transition Metal Hydrides. *Chem. Soc. Rev.* **2020**, *49*, 7929−7948.
(43) Handoo, K. L.; Cheng, J. P.; Parker, V. D. Hydride Affinities of Organic Radicals in Solution. A Comparison of Free Radicals and Carbenium Ions as Hydride Ion Acceptors. *J. Am. Chem. Soc.* **1993**, *115*, 5067−5072.
(44) Zhu, X.-Q.; Wang, C.-H.; Liang, H.; Cheng, J.-P. Theoretical Prediction of the Hydride Affinities of Various p- and o-Quinones in DMSO. *Journal of Organic Chemistry* **2007**, *72*, 945−956.
(45) Cheng, J.; Handoo, K. L.; Xue, J.; Parker, V. D. Free Energy Hydride Affinities of Quinones in Dimethyl Sulfoxide Solution. *Journal of Organic Chemistry* **1993**, *58*, 5050−5054.
(46) Ellis, W. W.; Raebiger, J. W.; Curtis, C. J.; Bruno, J. W.; DuBois, D. L. Hydricities of BzNADH, $C_5H_5Mo(PMe_3)(CO)_2H$, and $C_5Me_5Mo(PMe_3)(CO)_2H$ in Acetonitrile. *J. Am. Chem. Soc.* **2004**, *126*, 2738−2743.
(47) Brereton, K. R.; Jadrich, C. N.; Stratakes, B. M.; Miller, A. J. M. Thermodynamic Hydricity across Solvents: Subtle Electronic Effects and Striking Ligation Effects in Iridium Hydrides. *Organometallics* **2019**, *38*, 3104−3110.
(48) Mathis, C. L.; Geary, J.; Ardon, Y.; Reese, M. S.; Philliber, M. A.; Vanderlinden, R. T.; Saouma, C. T. Thermodynamic Analysis of Metal-Ligand Cooperativity of PNP Ru Complexes: Implications for CO_2 Hydrogenation to Methanol and Catalyst Inhibition. *J. Am. Chem. Soc.* **2019**, *141*, 14317−14328.
(49) Handoo, K. L.; Cheng, J. P.; Parker, V. D. Hydride Affinities of Organic Radicals in Solution. A Comparison of Free Radicals and Carbenium Ions as Hydride Ion Acceptors. *J. Am. Chem. Soc.* **1993**, *115*, 5067−5072.
(50) Ilic, S.; Alherz, A.; Musgrave, C. B.; Glusac, K. D. Thermodynamic and Kinetic Hydricities of Metal-Free Hydrides. *Chem. Soc. Rev.* **2018**, *47*, 2809−2836.
(51) Hargenrader, G. N.; Weerasooriya, R. B.; Ilic, S.; Niklas, J.; Poluektov, O. G.; Glusac, K. D. Photoregeneration of Biomimetic Nicotinamide Adenine Dinucleotide Analogues via a Dye-Sensitized Approach. *ACS Applied Energy Materials* **2019**, *2*, 80−91.
(52) Eisner, U.; Kuthan, J. Chemistry of Dihydropyridines. *Chem. Rev.* **1972**, *72*, 1−42.
(53) Walsh, C. Naturally Occurring 5-Deazaflavin Coenzymes: Biological Redox Roles. *Acc. Chem. Res.* **1986**, *19*, 216−221.
(54) Hiromoto, T.; Warkentin, E.; Moll, J.; Ermler, U.; Shima, S. The Crystal Structure of an [Fe]-Hydrogenase−Substrate Complex Reveals the Framework for H_2 Activation. *Angew. Chem., Int. Ed.* **2009**, *48*, 6457−6460.
(55) Brunet, P.; Wuest, J. D. Formal Transfers of Hydride from Carbon−Hydrogen Bonds. Generation of H_2 from Orthoformamides Designed To Undergo Intramolecular Protonolyses of Activated Carbon−Hydrogen Bonds. *Journal of Organic Chemistry* **1996**, *61*, 2020−2026.
(56) Wiberg, K. B.; Bailey, W. F.; Lambert, K. M.; Stempel, Z. D. The Anomeric Effect: It's Complicated. *Journal of Organic Chemistry* **2018**, *83*, 5242−5255.
(57) Rueping, M.; Sugiono, E.; Azap, C.; Theissmann, T.; Bolte, M. Enantioselective Brønsted Acid Catalyzed Transfer Hydrogenation: Organocatalytic Reduction of Imines. *Org. Lett.* **2005**, *7*, 3781−3783.
(58) Ouellet, S. G.; Walji, A. M.; Macmillan, D. W. C. Enantioselective Organocatalytic Transfer Hydrogenation Reactions Using Hantzsch Esters. *Acc. Chem. Res.* **2007**, *40*, 1327−1339.
(59) Zheng, C.; You, S.-L. Transfer Hydrogenation with Hantzsch Esters and Related Organic Hydride Donors. *Chem. Soc. Rev.* **2012**, *41*, 2498−2518.
(60) Yang, J. W.; List, B. Catalytic Asymmetric Transfer Hydrogenation of α-Ketoesters with Hantzsch Esters. *Org. Lett.* **2006**, *8*, 5653−5655.
(61) Rueping, M.; Antonchick, A. P.; Theissmann, T. A Highly Enantioselective Brønsted Acid Catalyzed Cascade Reaction: Organocatalytic Transfer Hydrogenation of Quinolines and Their Application in the Synthesis of Alkaloids. *Angew. Chem., Int. Ed.* **2006**, *45*, 3683−3686.
(62) Ouellet, S. G.; Tuttle, J. B.; MacMillan, D. W. C. Enantioselective Organocatalytic Hydride Reduction. *J. Am. Chem. Soc.* **2005**, *127*, 32−33.
(63) Yang, J. W.; Hechavarria Fonseca, M. T.; List, B. A Metal-Free Transfer Hydrogenation: Organocatalytic Conjugate Reduction of α,β-Unsaturated Aldehydes. *Angew. Chem., Int. Ed.* **2004**, *43*, 6660−6662.
(64) Bennett, L. E.; Warlop, P. Electron Transfer to Ozone: Outer-Sphere Reactivities of the Ozone/Ozonide and Related Non-Metal Redox Couples. *Inorg. Chem.* **1990**, *29*, 1975−1981.
(65) Hazari, N.; Heimann, J. E. Carbon Dioxide Insertion into Group 9 and 10 Metal-Element σ Bonds. *Inorg. Chem.* **2017**, *56*, 13655−13678.
(66) Wu, H.; Tian, C.; Song, X.; Liu, C.; Yang, D.; Jiang, Z. Methods for the Regeneration of Nicotinamide Coenzymes. *Green Chem.* **2013**, *15*, 1773−1789.
(67) Ilic, S.; Brown, E. S.; Xie, Y.; Maldonado, S.; Glusac, K. D. Sensitization of p-GaP with Monocationic Dyes: The Effect of Dye Excited-State Lifetime on Hole Injection Efficiencies. *J. Phys. Chem. C* **2016**, *120*, 3145−3155.

https://doi.org/10.1021/acs.accounts.1c00708
Acc. Chem. Res. 2022, 55, 844−856